Journal of Rock Mechanics and Geotechnical Engineering 18 (2026) 3904–3915

Contents lists available at ScienceDirect

Journal of Rock Mechanics and Geotechnical Engineering

journal homepage: www.jrmge.cn

Full Length Article

Measurement performance of six different actively-heated fiber-optic soil water content sensors: Numerical simulations and in situ applications

Mengya Sun [a], Juncheng Yao [b,*], Jie Liu [c], Jin Liu [a], Yuling Xin [a], Bin Shi [c,**]

[a] School of Earth Sciences and Engineering, Hohai University, Nanjing, 210098, China
[b] Department of Architecture and Civil Engineering, City University of Hong Kong, 999077, Hong Kong, China
[c] School of Earth Sciences and Engineering, Nanjing University, Nanjing, 210023, China

ARTICLE INFO

Article history:
Received 8 January 2025
Received in revised form
3 June 2025
Accepted 10 June 2025
Available online 24 September 2025

Keywords:
Soil water content
Actively-heated fiber-optic (AHFO) sensor
Measurement properties
In situ application
Monitoring potential

ABSTRACT

The actively-heated fiber-optic (AHFO) method can near-continuously measure soil water content along the AHFO sensors by sensing the temperature variation during an actively heated pulse. Different heating materials, structures, and fiber-optic temperature sensing techniques significantly impact the measurement performance of AHFO sensors. However, there has been no systematic evaluation regarding the measurement performance of soil water content by different AHFO sensors. To address this issue, this study focuses on the measurement performance and monitoring potential of six different AHFO sensors (i.e. actively-heated fiber Bragg grating (AH-FBG) alundum tube, AH-FBG cable, carbon fiber heated cable (CFHC), copper metal heated cable (CMHC), CFHC sensing tube, and CMHC sensing tube). Numerical models were built first for simulating the thermal response process of six AHFO sensors to quantify the measurement accuracy and sensitivity of soil water content. Then, the in situ applications of six AHFO sensors were carried out in Yan'an, China. The numerical and in situ monitoring results indicate that the measurement accuracy and sensitivity of soil water content are both highest by using CFHC sensing tube and CMHC sensing tube. CMHC sensing tube is most suitable for fine and accurate monitoring of in situ soil, while AH-FBG alundum tube and AH-FBG cable are best suited for long-term real-time remote monitoring. In practical applications, it is recommended that geotechnical engineers, when selecting AHFO sensors for a specific site project, should take into account a variety of factors, including measurement performance, spatial resolution, monitoring duration, site installation, and power supply conditions.

1. Introduction

The soil water content, a fundamental physical parameter of soil, reflects the mechanical and hydrological properties of soil (e.g. Taylor and Cavazza, 1954; Heitman et al., 2008; Liu et al., 2023). Hence, accurately acquiring the variation of soil water content is an important task for revealing the water-heat interaction between soil and atmosphere in environmental and geotechnical engineering (e.g. Bittelli et al., 2008; Liu et al., 2024a). Fiber-optic sensors garnered extensive research interest in recent decades (e.g. Bao et al., 2019; Qin et al., 2022). With the advantage of high sensitivity, real-time monitoring, and excellent corrosion resistance (e.g. Striegl and Loheide II, 2012; Yao et al., 2022; Zhang et al., 2023), its capacity of measuring temperature and assessing moisture exhibits a strong performance (e.g. Bao and Chen, 2016). Among various fiber-optic methods, the actively-heated fiber-optic (AHFO) method, fast developing over the past decade, has been widely used for in situ measurement of soil water content (e.g. Sayde et al., 2010; Sun et al., 2021; Liu et al., 2024b). It has been well recognized that AHFO method can provide the near-continuous spatial distribution of the soil water content along the AHFO sensors, allowing researchers to effectively capture fine-

* Corresponding author.
** Corresponding author.
E-mail addresses: jcyao2-c@my.cityu.edu.hk (J. Yao), shibin@nju.edu.cn (B. Shi).

Peer review under responsibility of Institute of Rock and Soil Mechanics, Chinese Academy of Sciences.

https://doi.org/10.1016/j.jrmge.2025.06.043

scale variations in soil water content (e.g. Sayde et al., 2010; Sun et al., 2024a).

The fundamental principle of AHFO method is that the AHFO sensor is capable of simultaneously releasing heat and measuring the real-time temperature variations during the heating process (e.g. Ciocca et al., 2012). Due to the soil thermal properties changing with the soil water content (e.g. Kluitenberg et al., 1993; Bristow et al., 1994), the temperature variation process is highly correlated with the soil water content. This strong correlation can be used to estimate the soil water content along the AHFO sensor from the measured temperature variation. Before the measurement, the relationship between the soil water content and temperature variation measured by different AHFO sensors needs to be calibrated. Several calibration methods have been developed for AHFO sensors to estimate soil water content, including the temperature characteristic value (T_t) method, cumulative temperature increase (T_{cum}) method, and thermal conductivity (λ) method (e.g. Striegl and Loheide II, 2012; Cao et al., 2015; Benítez-Buelga et al., 2016; Wang et al., 2020). Among these calibration methods, the temperature characteristic value (T_t) method has emerged as the mainstream approach due to its simplicity and efficiency. However, under identical heating conditions, the calibrated relationship may vary when different AHFO sensors are employed. That is because the heat conduction process might be changed by different heating materials and structures of AHFO sensors.

Recently, a considerable amount of research has employed AHFO sensors for soil water content measurement (e.g. Gil-Rodríguez et al., 2013; Sayde et al., 2015; Sourbeer and Loheide, 2016; Wu et al., 2023; Sun et al., 2024a). However, the AHFO sensors used by different researchers exhibit significant differences, with variations in fiber optic temperature sensing technologies, sensor structures, and heating materials. In terms of fiber optic sensing technology, temperature sensing technologies such as distributed temperature sensing (DTS) and fiber Bragg grating (FBG) are commonly employed in AHFO sensors, respectively, i.e. actively heated DTS (AH-DTS) sensors and actively heated FBG (AH-FBG) sensors (e.g. Sayde et al., 2014; Sun et al., 2020; Zhang et al., 2020; Wu et al., 2021; Li et al., 2023). Note that the temperature measurement accuracy varies with different fiber optic temperature sensing technologies. This may further impact the measurement accuracy of soil water content. In terms of sensor structure, all AHFO sensors can be divided into two main types: cable-shape sensors and tube-shape sensors (e.g. Cao et al., 2016; Liu et al., 2024a; Sun et al., 2024a). Cable-shape sensors include different types of AHFO cables, e.g. actively heated fiber Bragg grating (AH-FBG) cable, carbon fiber heated cable (CFHC), and copper mesh heated cable (CMHC). Tube-shape sensors include CFHC sensing tube, CMHC sensing tube and AH-FBG alundum tube. CFHC sensing tube and CMHC sensing tube are made from AHFO cables, i.e. CFHC and CMHC, respectively. In terms of heating materials, the common heating materials used in AHFO sensors include metal wire, metal mesh, and carbon fiber (e.g. Cao et al., 2016; Yao et al., 2022; Li et al., 2023; Sun et al., 2024b). However, different sensor structures and heating materials can affect the thermal diffusion process of the AHFO sensor, further impacting the measurement performance of soil water content measurement. Based on the aforementioned analysis, it can be concluded that different AHFO sensors have different measurement properties and potential for soil water content measurement. In other words, the differences in temperature measurement accuracy, sensor materials, and structures among various types of sensors lead to variations in the water content measurement performance and application scenarios of each type of sensor. The current application of AHFO sensors reveals a significant research gap, particularly the lack of a comprehensive and systematic evaluation of different AHFO sensors, along with corresponding application standards and monitoring potential. This deficiency in performance characterization presents substantial challenges for rational sensor selection and field application, thereby hindering the broader adoption of AHFO sensors for soil water content monitoring. Therefore, a comparative analysis of sensor-specific influences on the quantitative measurement performance of AHFO-based soil water content measurements is imperative.

To address these limitations, this study focuses on the measurement performance and potential comparison of six different AHFO sensors. Numerical simulations and in situ measurements are conducted for each of the six AHFO sensors in this study. For fair comparison, the effect of different AHFO sensors on the measurement accuracy and sensitivity is investigated in numerical simulations, with consideration of the measurement accuracy of temperature. In addition, the in situ measurements are used to evaluate the real performance of different AHFO sensors. Finally, the measurement properties and monitoring potential of different AHFO sensors are summarized to provide a reference for their further application.

2. Soil water content measurement by AHFO sensors

This section delineates the methodology for soil water content measurement using AHFO sensors, structured into three key components. First, the technical specifications of six self-developed AHFO sensors are characterized in detail. Second, the underlying thermodynamic principles governing soil water content estimation via AHFO sensors are elucidated, emphasizing the relationship between temperature variation and soil water content. Finally, laboratory and field calibration procedures are outlined, ensuring robust alignment of sensor outputs with ground-truth.

2.1. AHFO sensors

Currently, there are six types of self-developed AHFO sensors by authors' research group, including AH-FBG alundum tube, AH-FBG cable, CFHC, CMHC, CFHC sensing tube, and CMHC sensing tube. Table 1 shows the actual photos and main characteristics of these six AHFO sensors.

The temperature measurement of AHFO sensors can be summarized into two categories: DTS technology and FBG technology. The DTS technology is based on the Raman scattering effect to measure temperature and is positioned by the time domain reflection technique of light. While the FBG measures temperature by detecting the shift in backscattered Bragg wavelength. Technically, CFHC, CMHC, CFHC sensing tube, and CMHC sensing tube are sensors based on DTS with a temperature measurement accuracy of 0.3 °C; both AH-FBG alundum tube and AH-FBG cable are based on FBG with a temperature measurement accuracy of 0.1 °C.

In terms of sensor shape, AH-FBG alundum tube, CFHC sensing tube, and CMHC sensing tube are tube-shaped sensors, cylindrical in shape with a certain rigidity and not easily bendable; AH-FBG cable, CFHC, and CMHC are cable-shaped sensors, linear in shape with good flexibility and bendability. It is important to note that the CFHC sensing tube is formed by winding CFHC around a PVC tube, and the CMHC sensing tube is created by winding CMHC around a wire hose. However, the spatial resolution of the two types of sensing tubes (about 0.035 m) has significantly improved compared to that of the corresponding DTS cables (1 m), which is the main difference between cable-shaped and tube-shaped AH-DTS sensors. In addition, the heating material and diameter of six AHFO sensors are different, as detailed in Table 1. It is obvious that CFHC sensing tube and CMHC sensing tube have a larger diameter than other AHFO sensors.

Table 1
Six AHFO sensors and their characteristics.

Sensor type		Sensor shape	Heating material	Diameter (cm)	Fiber-optic sensing technology
AH-FBG cable		Cable shape	Metal net	0.5	FBG
AH-FBG alundum tube		Tube shape	Metal wire	0.7	
CFHC		Cable shape	Carbon fiber	0.42	DTS
CMHC		Cable shape	Metal net	0.53	
CFHC sensing tube	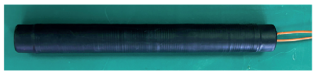	Tube shape	Carbon fiber	5.84	
CMHC sensing tube		Tube shape	Metal net	5.25	

2.2. Principle of soil water content measurement

The AHFO sensor buried in the soil can be regarded as an infinite cylindrical heat source. Based on the principle of infinite cylindrical heat source, after the AHFO sensor is heated for a certain time, the temperature-time curve measured by the sensor can be expressed as (Ciocca et al., 2012):

$$T_t = T(t) - T_0 = \frac{Q}{4\pi\lambda}\left[\ln t + 4\pi R\lambda + \ln\left(\frac{4K}{a^2 c}\right)\right] \quad \left(t \gg a^2 \Big/ K\right) \tag{1}$$

where T_t is the temperature characteristic value (°C), $T(t)$ is the temperature of the heat source (°C) corresponding to the heating time (t), T_0 is the initial soil temperature (°C), Q is the heating power per unit length (W m^{-1}), λ is the thermal conductivity of the soil (W m^{-1} K^{-1}), R is the soil-sensor thermal contact resistance per unit length (m K W^{-1}), K is the thermal diffusivity (m^2 s^{-1}) of the soil, a is the outer diameter (m) of the sensor, and $c = 1.7811 = \exp(\gamma)$ in which γ is the Euler–Mascheroni constant ($\gamma = 0.5772$).

Sayde et al. (2010) first proposed that there was a unique and monotonic T_t–θ relationship for a certain type of soil. Therefore, the θ profile can be determined based on the T_t profile. Note that the T_t–θ calibration curve should be established before measurements. The T_t-θ calibration model used in this study is (Sun et al., 2020):

$$T_t = \frac{1}{A\theta/(1 + B\theta) + C} \tag{2}$$

where θ is the soil volumetric water content (m^3 m^{-3}); and A, B and C are fitting parameters determined by the calibration test.

Therefore, according to the T_t-θ relationship calibrated in advance, the θ can be calculated according to the T_t measured from AHFO sensors:

$$\theta = \frac{1/T_t - C}{A + BC - B/T_t} \tag{3}$$

2.3. Calibration process

Before the soil water content measurement by AHFO sensors, the relationship between T_t and θ need to be calibrated. The calibration methods are categorized into laboratory and in situ calibration.

For laboratory calibration, AHFO sensors are embedded in soil samples with predefined water content gradients, followed by heating and recording of corresponding T_t values (e.g. Sun et al., 2020). Note that the prepared samples with different soil water contents are usually sealed with plastic wrap individually, standing for 24 h to ensure the homogeneous distribution of water. After the heating test, to assess possible evaporation, the oven-drying method is used to measure the water content of taken soil samples. If the difference between final water content and initial water content is within 0.5 %, it can be believed that there is no significant evaporation in the soil samples. A calibration equation (i.e. Eq. (2)) is derived by nonlinearly fitting the T_t-θ relationship.

In situ calibration, as opposed to laboratory calibration, directly utilizes the in situ soil at a specific site, potentially improving the calibration accuracy. Unlike the oven-drying method used in laboratory calibration, point-specific techniques (e.g. time domain reflectometry (TDR), and neutron probe tube method) are employed to measure water content as ground truth in deep soil layers (e.g. Sun et al., 2024b). Notably, in situ calibration cannot preset the desired θ need to be calibrated. Instead, water content gradients are altered either artificially (e.g. through watering) or via natural evaporation, thereby reflecting realistic variations in θ. Additionally, site-specific soil properties, which is difficult to replicate in laboratories, enhance field applicability of in situ calibration. Following the same nonlinear fitting as laboratory calibration, Eq. (2) is obtained to derive the calculation formula (i.e. Eq. (3)).

3. Test methods

In this study, numerical simulations and in situ applications are

both conducted to evaluate the measurement performance of six AHFO sensors. Initially, six numerical models were developed to simulate soil water content calibration and measurement processes, enabling an equitable comparison of the sensors under controlled and idealized conditions. Subsequently, all six AHFO sensors were deployed at the same field site to assess their performance in real-world environmental settings. The test methods are detailed as follows.

3.1. Numerical simulation model

For calibration and further analysis, the numerical simulation models of six AHFO sensors were built in a Multiphysics finite-element method (FEM) software, as shown in Fig. 1. Here, homogeneous conditions along the direction of the cable are assumed, with the problem simplified into two spatial dimensions (e.g. Benítez-Buelga et al., 2016). Fig. 1a shows the location of sensor in the soil, with the specific location at the center of 1 m × 1 m soil. Fig. 1b-e shows the structure of six AHFO sensors in detail, respectively. Note that the scale bar of Fig. 1b–f differs from that of Fig. 1e and g because of the different scales of sensors.

The thermal parameters for numerical models of different AHFO sensors are summarized in Table 2. Firstly, the initial temperatures of all materials in the numerical models before heating are set the same as 10 °C (i.e. 283.15 K). For most numerical models of AHFO sensors, a heat pulse of 15 W m^{-1} lasting 1200 s was simulated, as this duration ensures attainment of stable heat transfer stage within the soil (e.g. Yao et al., 2023). It is well noted that the heating powers for 1 m CFHC sensing tube and CMHC sensing tube are not equal to 15 W m^{-1} (i.e. heating power per meter) because CFHC sensing tube and CMHC sensing tube are made of CFHC and CMHC twining the tube. For fair comparison in further analysis, the heat pulses for CFHC sensing tube and CMHC sensing tube are set as 10 W m^{-1} and 15 W m^{-1}, all corresponding to 376 W for 1 m CFHC sensing tube and CMHC sensing tube, respectively.

The calibration of different AHFO sensors needs to simulate the heat pulse process in the soils with different water contents repeatedly. In this study, five soils with different water contents (i.e. soil I, II, III, IV, and V) are used for calibration. The physical parameters of five soils are summarized in Table 3, obtained from the laboratory experiments using soil samples. The soil samples used in this study were sampled from the study site in the next subsection. The mass water content and dry density were measured using the oven-drying method, and then the volumetric soil water content and density of soil samples can be calculated. Moreover, the specific heat capacity of soil solid is determined by the differential calorimetric scanning (DSC) method in advance, i.e. 750 J kg^{-1} K^{-1}. Hence, the soil volumetric heat capacity and constant pressure heat capacity can be calculated based on that. In addition, the soil thermal conductivity was determined by the steady-state plate method (HC-110, EKO, Japan). In addition, the material parameters used in this numerical experiment are consistent with those before (e.g. Yao et al., 2023).

3.2. In situ study site

The in situ study site is located on a loess beam (36°47′22.69″N, 109°49′05″E) in Ganguyi Town, Yan'an City, Shaanxi Province, China. The geographic location of the study site is shown in Fig. 2a. A test pit, with a diameter of 1 m and a depth of 29.56 m, was manually excavated in the study site, as shown in Fig. 2b. Six AHFO sensors, the same as Section 3.2, were deployed in the test pit, as shown in Fig. 2c. It is important to note that different AHFO sensors were installed at varying depths within the test pit. This arrangement was necessitated by a combination of site conditions, installation difficulties, and the distinct characteristics of each type of AHFO sensor.

The layout of different sensors in test pit, including AH-FBG alundum tube, AH-FBG cable, CMHC sensing tube, CFHC sensing tube, CMHC, CFHC, and neutron probe access tube, are introduced in detail as follows. The first three AH-FBG alundum tubes are located from 0 m to 1.41 m next to each other, and the other six AH-FBG alundum tubes are located at the depths of 3.35 m, 4.35 m, 10.35 m, 16.35 m, 22.35 m, and 29.35 m, respectively. Each AH-FBG alundum tube, with a length of 0.47 m, has four measurement points, located at an equal interval of 10 cm. Two AH-FBG cables are located from 0 m to 9.1 m and 13.1 m–22.1 m, respectively, both with the interval between each FBG measurement points of 1 m. Due to poor etching quality of the FBG at 18.1 m, which resulted in weak reflection signals, this FBG measurement point was excluded from further analysis. Owing to the high electrical resistance of

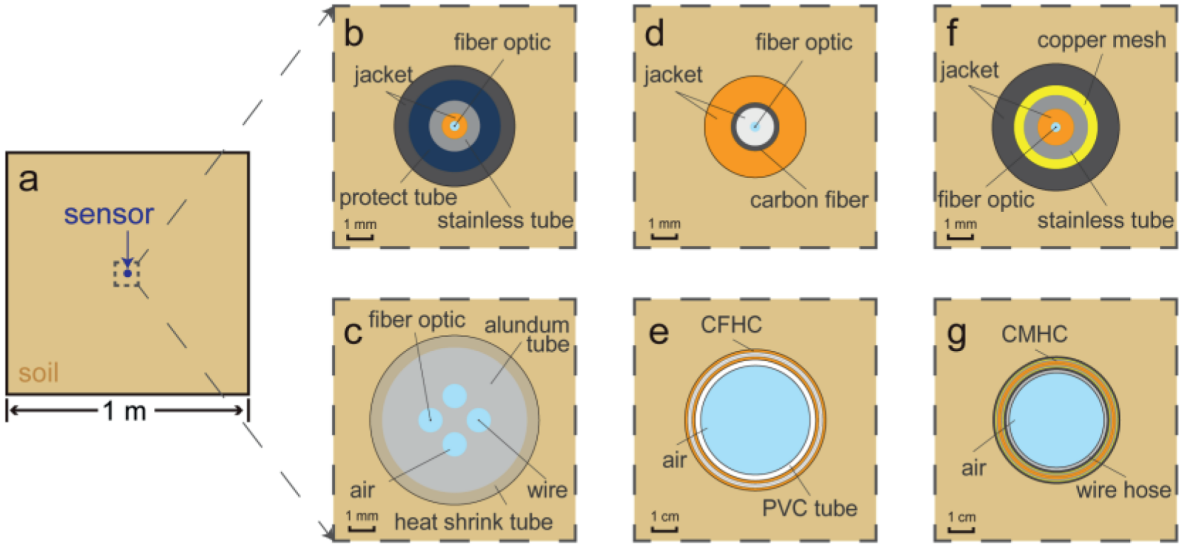

Fig. 1. Numerical simulation models of six AHFO sensors: (a) Sensor location in the soil, (b) AH-FBG cable, (c) AH-FBG alundum tube, (d) CFHC, (e) CFHC sensing tube, (f) CMHC, and (g) CMHC sensing tube.

Table 2
Thermal parameters for numerical models of different AHFO sensors.

Sensor	Initial temperature (°C)	Heating duration (s)	Heating power per meter (W)	Total heating power for 1 m sensor (W)
AH-FBG cable	10	1200	15	15
AH-FBG alundum tube	10	1200	15	15
CFHC	10	1200	15	15
CMHC	10	1200	15	15
CFHC sensing tube	10	1200	10	376
CMHC sensing tube	10	1200	15	376

Table 3
Physical parameters of soils used in numerical models.

Soil	Mass water content (kg/kg)	Dry density (kg/m^3)	Density (kg/m^3)	Volumetric water content (m^3/m^3)	Volumetric heat capacity (kJ/(m^3 K))	Constant pressure heat capacity (kJ/(kg K))	Thermal conductivity (W/(m K))
I	0.1851	1410.8	1672	0.2612	2.1499	1.2858	1.206
II	0.1479	1403.6	1611.2	0.2077	1.9207	1.1921	1.095
III	0.1024	1401.3	1544.8	0.1435	1.6509	1.0686	0.9442
IV	0.0902	1404.1	1530.7	0.1266	1.5824	1.0337	0.879
V	0.0519	1393.8	1466.2	0.0724	1.3479	0.9193	0.6751

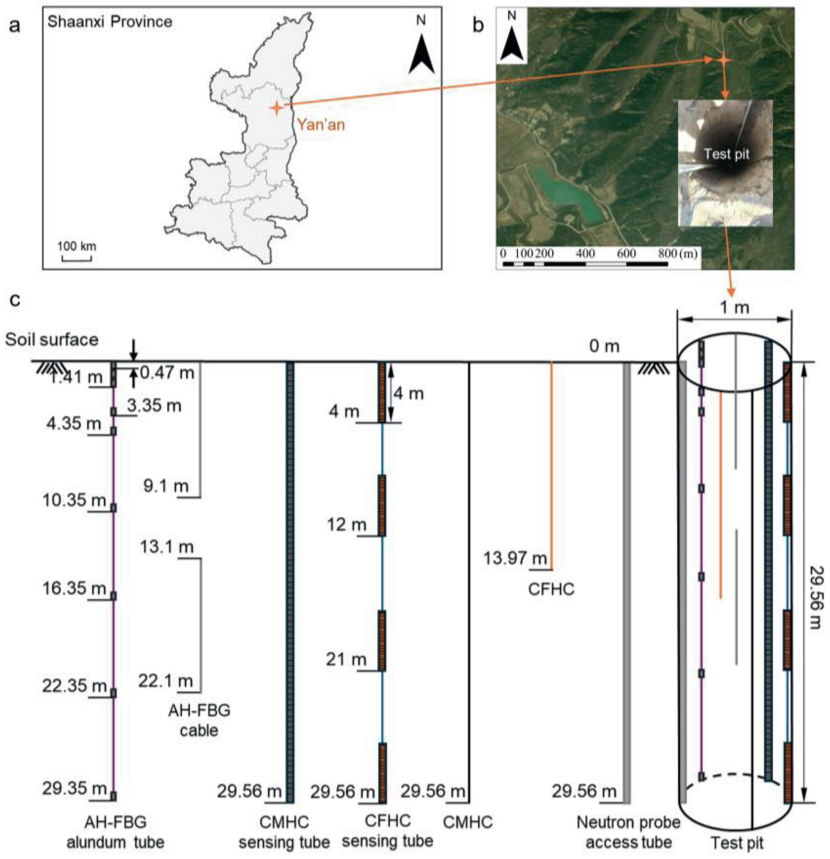

Fig. 2. Geographic location and layout of AHFO sensors: (a) Geographic location of study site, (b) Location of test pit, and (c) Layout scheme of sensors in test pit.

carbon fiber in CFHC and CFHC sensing tubes, in order to achieve sufficient heating power per meter, the CFHC and each CFHC sensing tube were limited to lengths of 13.97 m and 4 m, respectively. Four CFHC sensing tubes are located from 0 m to 4 m, from 8 m to 12 m, from 17 m to 21 m, and from 25.56 m to 29.56 m, respectively. The CMHC and CMHC sensing tubes are both 29.56 m in length, touching the bottom of the test pit. In consideration of the sensor resistance and on-site power supply conditions, the heating voltages were set as follows: 24 V for AH-FBG alundum tube and AH-FBG cable, 22 V for CMHC, 220 V for CMHC sensing tube and CFHC, and 110 V for CFHC sensing tube. Note that each heating lasts 20 min for each sensor, at most once a day, to avoid the potential water migration by frequent heating-cooling cycles (e.g. Guo et al., 2020). In addition, for the calibration and validation of the measured soil water content, a neutron probe access tube was also installed in the test pit, extending from the soil surface to the depth of 29.56 m.

4. Results and discussion

4.1. T_t-θ calibration results in numerical simulations

To compare the T_t-θ calibration results of AHFO sensors, the numerical models simulate the same heating pulse in AHFO sensors for soils with different water contents. Numerical simulations were conducted on five soils proposed in Section 3.2, while the real-time temperature variation of the fiber optic was measured during the heating pulse. The calibration curves shown in Fig. 3 are determined after fitting the T_t measured from different AHFO sensors with the θ.

It is observed from Fig. 3 that the fitting curves perform well with high fitting correlation coefficients, indicating that the hating process in numerical simulations is very close to reality. Table 4 provides a detailed list of the calibration results of six AHFO sensors in numerical simulations. It is worth noting that the fitting correlation coefficients R^2 of these sensors are all above 0.999, very close to 1. This indicates that the calibration results obtained from this numerical simulation are in agreement with the calibration formula derived from the theoretical model. Moreover, it validates that this numerical model can be employed for further analysis of soil water content measurement results.

The temperature characteristic values T_t measured from different AHFO sensors in Fig. 3 range from high to low in the following order: CFHC sensing tube, CMHC sensing tube, CFHC, AH-FBG cable, CMHC, and AH-FBG alundum tube. This is due to the different sizes of the sensors and different physical properties of materials. For fair comparison of the temperature variation process, Fig. 4 shows the temperature rise curves of different AHFO sensors in the same soil (i.e. soil II). To facilitate differentiation, the six sensors are divided into small-diameter sensors (i.e. CMHC, CFHC, AH-FBG cable, and AH-FBG alundum tube in Fig. 4a) and large-diameter sensors (i.e. CFHC sensing tube and CMHC sensing tube in Fig. 4b) based on their size scales. The two large-diameter sensors (i.e. CFHC sensing tube and CMHC sensing tube) are both made of cables twining the tubes, and the heating powers for 1 m sensors are different from that of the small-diameter sensors, as mentioned in Section 3. Therefore, their temperature characteristic values are much higher than those of the small-diameter sensors. Moreover, the difference of materials in different AHFO sensors is another important factor on the difference of temperature rise curves using different AHFO sensors. For example, CFHC and CMHC share the similar structure and size, but the high heat capacity of stainless tube in CMHC causes the lower T_t than that of CFHC (e.g. Yao et al., 2023). The high or low T_t may influence the measurement performance of soil water content using different AHFO sensors, as discussed in the next subsection. In addition, the authors' research group has investigated the accuracy of the numerical calibration results of CFHC and CMHC, and found that the numerical calibration results are consistent with the actual laboratory calibration results, verifying the reliability of the numerical model (e.g. Yao et al., 2023).

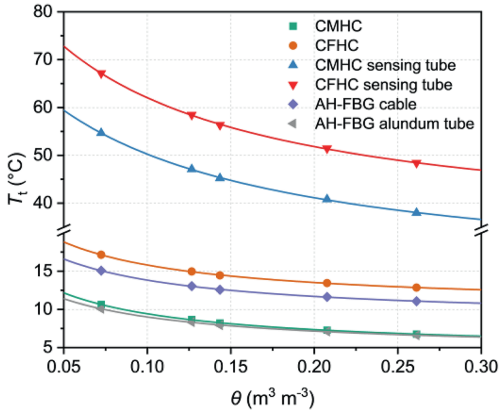

Fig. 3. Calibration curves of different AHFO sensors determined by numerical simulation.

Table 4
Calibration results of numerical simulation using different AHFO sensors.

Sensor	A	B	C	R^2
CMHC	0.88898	4.95124	0.0466	0.99932
CFHC	0.53062	8.42844	0.03445	0.99913
CMHC sensing tube	0.09217	3.02163	0.01282	0.99946
CFHC sensing tube	0.07997	3.99107	0.0104	0.99958
AH-FBG cable	0.5899	7.65611	0.03888	0.99923
AH-FBG alundum tube	0.87964	5.11425	0.05274	0.99926

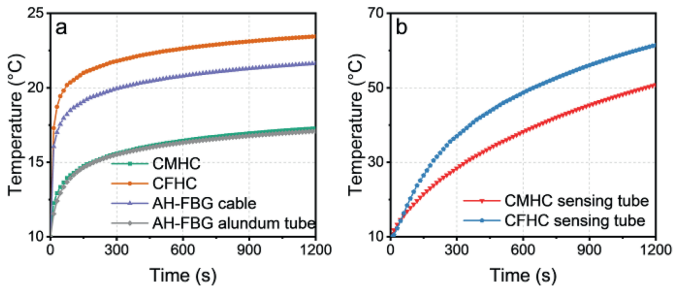

Fig. 4. Temperature rise curve measured from different AHFO sensors in soil II: (a) Small-diameter sensors, and (b) Big-diameter sensors.

4.2. Measurement performance of soil water content in numerical simulations

4.2.1. Measurement accuracy

In this section, the impact of the calibration on water content measurement results is quantified in the numerical simulation. One important limitation of numerical simulation is in an ideal condition, meaning that the measured temperature is accurate without any measurement error or noise. However, in real-world applications, the measurement accuracy of temperature is one of most important impact on soil water content measurement using AHFO sensors. Considering the measurement accuracy of temperature, the formula for the measurement accuracy of soil water content from calibration formula is derived as follows. Firstly, by taking the derivative of θ with respect to T_t in Eq. (3), the following equation can be obtained:

$$\frac{\mathrm{d}\theta}{\mathrm{d}T_t} = -\frac{A}{[(A+BC)T_t - B]^2} \tag{4}$$

The relationship between the measurement accuracy of soil water content ($\Delta\theta$) and the measurement accuracy of temperature characteristic value (ΔT_t) (i.e. measurement accuracy of temperature) can be expressed as follows:

$$\Delta\theta = \pm\sqrt{\left(\frac{\mathrm{d}\theta}{\mathrm{d}T_t}\right)^2 \Delta T_t^2} \tag{5}$$

Substituting Eq. (4) into Eq. (5), the measurement accuracy of soil water content ($\Delta\theta$) is obtained as

$$\Delta\theta = \pm\frac{A}{[(A+BC)T_t - B]^2}\Delta T_t \tag{6}$$

Considering the $\Delta\theta$, the calculation formula of θ can be obtained as follows:

$$\theta(T_t) = \frac{1/T_t - C}{A + BC - B/T_t} \pm \frac{A}{[(A+BC)T_t - B]^2}\Delta T_t \tag{7}$$

Because the measurement accuracy of temperature by DTS sensors is 0.3 °C, and that by FBG sensors is 0.1 °C, substituting the calibration results from Table 3 into Eq. (7), the calculation formulae of θ and measurement accuracy using different AHFO sensors are shown in Fig. 5. Fig. 5 illustrates the calculation formula of θ and measurement accuracy using different AHFO sensors in numerical simulation. A comparison of all six AHFO sensors reveals that the two AH-FBG sensors (i.e. AH-FBG cable and AH-FBG alundum tube) perform well on measurements of soil water content due to their higher measurement accuracy of temperature by FBG sensors (i.e. 0.1 °C). In addition, the two DTS sensing tubes (i.e. CFHC sensing tube and CMHC sensing tube) have better performance than the DTS cables (i.e. CFHC and CMHC).

To further quantify the differences between measurement accuracy of the six AHFO sensors, the water content measurement accuracy at $\theta = 0.15$ m^3 m^{-3} is compared and presented as a bar graph in Fig. 6. It is obvious that the six AHFO sensors can be categorized into three groups: two traditional DTS cables (i.e. CMHC and CFHC), two DTS sensing tubes (i.e. CMHC sensing tube and CFHC sensing tube), and two AH-FBG sensors (i.e. AH-FBG cable and AH-FBG alundum tube). The two DTS sensing tubes exhibit the highest measurement accuracy due to their higher heating power per meter compared to other sensors. Meanwhile,

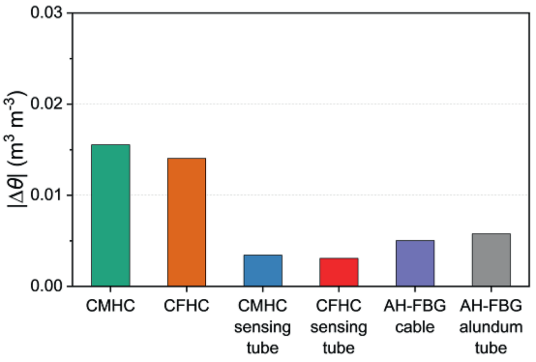

Fig. 6. Absolute value of measurement accuracy using different AHFO sensors at θ of 0.15 m^3 m^{-3}.

the two AH-FBG sensors perform better than traditional DTS cables, primarily because of their superior temperature measurement accuracy. Each group consists of two AHFO sensors with different materials, but similar structures and same fiber-optic temperature measurement technique, resulting in similar measurement accuracy of water content by these two AHFO sensors. Through comparison, it is evident that the main factors affecting measurement accuracy are structure of sensors and measurement accuracy of temperature, while the sensor material has a minor impact on measurement accuracy of soil water content.

4.2.2. Measurement sensitivity

In addition, it is necessary to evaluate the measurement performance of different AHFO sensors from the perspective of

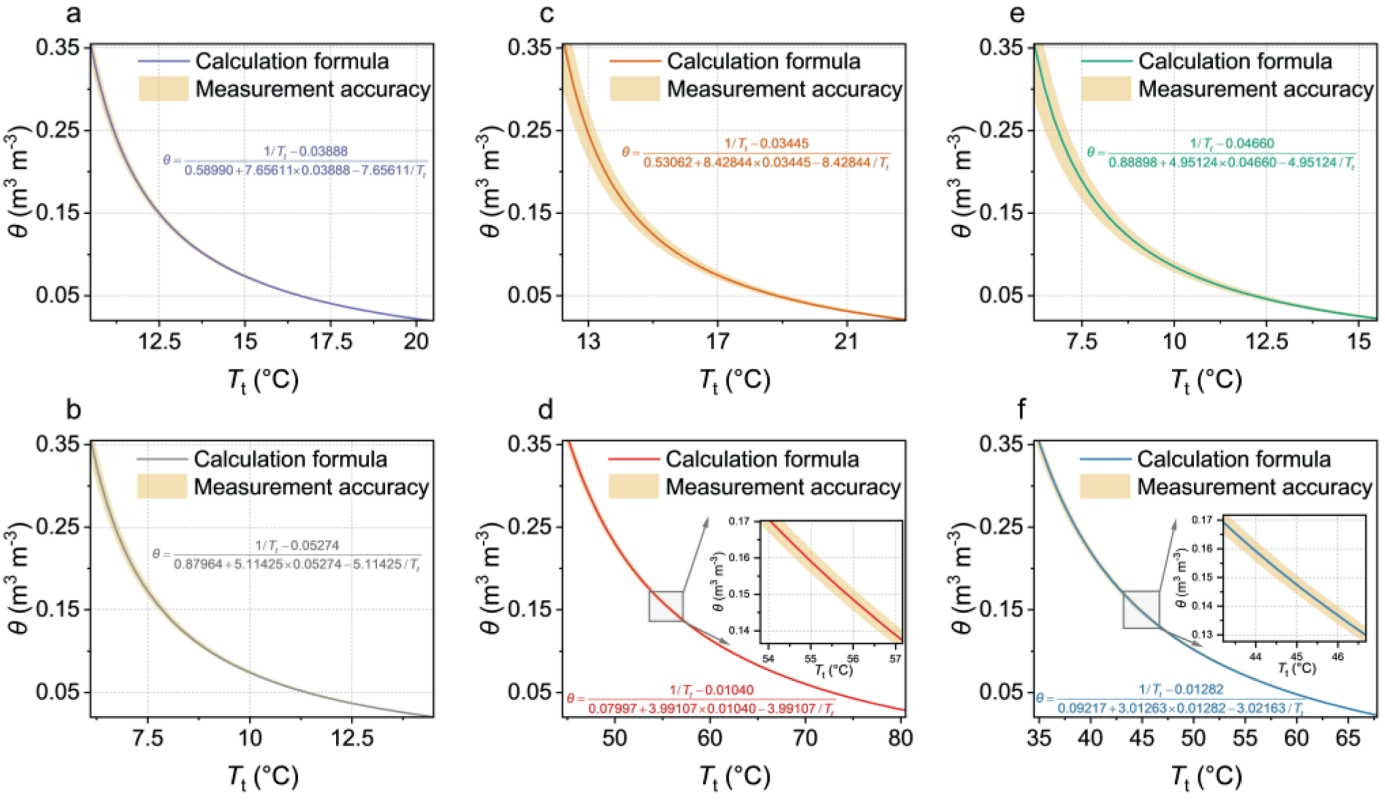

Fig. 5. Calculation formula of θ and measurement accuracy using different AHFO sensors: (a) AH-FBG cable, (b) AH-FBG alundum tube, (c) CFHC, (d) CFHC sensing tube, (e) CMHC, and (f) CMHC sensing tube.

measurement sensitivity. Measurement sensitivity for AHFO sensors is defined as the temperature change induced by a unit change in soil water content, i.e. the absolute value of the slope of the T_t-θ curve. A higher temperature change value caused by a unit change in soil water content indicates greater measurement sensitivity of the AHFO sensor, making it more capable of detecting subtle variations in soil water content. The expression for sensitivity is given by

$$\left|\frac{\mathrm{d}T_t}{\mathrm{d}\theta}\right| = \frac{|A|}{[(A+BC)\theta + C]^2} \tag{8}$$

where $|\mathrm{d}T_t/\mathrm{d}\theta|$ is the measurement sensitivity for AHFO sensors, and the "$|\cdot|$" brackets represent the absolute value.

The $|\mathrm{d}T_t/\mathrm{d}\theta|$-$\theta$ curves are shown in Fig. 7. The sensitivity value $|\mathrm{d}T_t/\mathrm{d}\theta|$ is calculated based on the T_t-θ calibration results in the numerical simulation as shown in Fig. 3 and Table 4, indicating the temperature variation per unit change in soil water content. A higher sensitivity value implies greater measurement sensitivity, while a lower value indicates lower sensitivity. In general, the two DTS sensing tubes show higher measurement sensitivity, enabling them to detect subtle changes in soil water content. The other four types of sensors exhibit relatively lower measurement sensitivity, although the differences are not substantial. Therefore, the measurement sensitivity of different AHFO sensors to perceive changes in soil water content varies.

To further quantify the differences in measurement sensitivity of the six AHFO sensors, the water content measurement sensitivity at $\theta = 0.15$ m^3 m^{-3} is compared and presented as a bar graph in Fig. 8. It is obviously shown that the six AHFO sensors can be categorized into two groups: two DTS sensing tubes, and the other four AHFO sensors. For two DTS sensing tubes, CFHC sensing tube is more sensitive to the slight variation of soil water content than CMHC sensing tube. For the other four AHFO sensors, the sensitivity from high to low is as follows: CFHC, AH-FBG cable, CMHC, AH-FBG alundum tube. Although the differences of these four AHFO sensors in measurement sensitivity are not significant, this information provides important reference for practical applications. In the next subsection, the in situ measurement performance of different AHFO sensors will be evaluated, respectively.

4.3. In situ measurement results

The numerical simulation is under an ideal condition without considering the measurement errors caused by soil moisture migration during the heat pulse process or the measurement noise

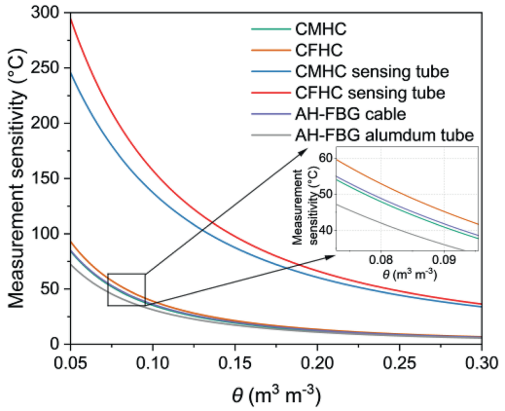

Fig. 7. Measurement sensitivity of soil water content measured by different AHFO sensors.

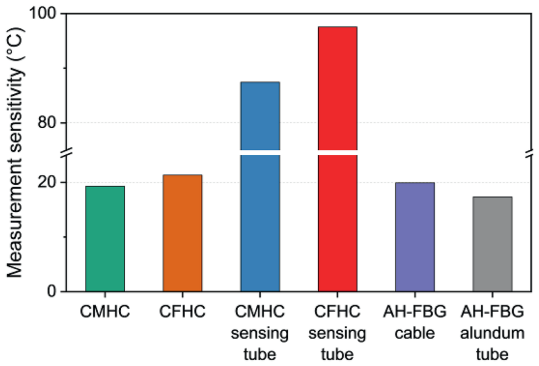

Fig. 8. Measurement sensitivity of different AHFO sensors at θ of 0.15 m^3 m^{-3}.

of temperature. Thus, it is necessary to compare the in situ performance of six AHFO sensors in in situ applications. The calibration results of in situ measurements are different from the ideal conditions in numerical simulations. For in situ calibrations, in situ measurements of different AHFO sensors were conducted with the measurements by neutron probe access tube sensor at the same locations. The in situ calibration results are summarized in Table 5. The calibration curves of in situ results for different AHFO sensors are shown in Fig. 9.

Utilizing the aforementioned calibration results, the in situ measurement in the test pit (i.e. as illustrated in Fig. 2) by different AHFO sensors was conducted along the depth direction at the same day (i.e. 28 June 2019). The measurement results are presented in Fig. 10. In general, the spatial distribution of θ measured from different AHFO sensors shares the same trend along the depth direction. Given that soil is a complex engineering material, the soil properties usually vary spatially with a varying trend and deviation from trend, i.e. so-called inherent soil variability (Phoon and Kulhawy, 1999). As shown in Fig. 10d and f, two DTS sensing tubes (i.e. CMHC sensing tube and CFHC sensing tube) can provide the inherent variability of measured soil water content most continuously with the sampling interval of about 0.014 m. However, the two DTS cables (i.e. CMHC and CFHC) only provided the near-continuous trend of spatial variability of measured soil water content without deviation from trend, as shown in Fig. 10c and e, because the sampling interval is only about 0.41 m. While the FBG measurement is a quasi-distribution sensing technique, two AH-FBG sensors only provided information of discretized measurements at specific locations of sensors, as shown in Fig. 10a and b. In addition, it is worth noting that both CFHC and CFHC sensing tubes are difficult to heat over long distances due to the high resistance of the carbon fiber (i.e. 18 Ω m^{-1}), which imposes a spatial limitation in their measurement length, as shown in Fig. 10c and d.

In addition, the FBG demodulator for the two AH-FBG sensors (i.e. AH-FBG cable and AH-FBG alundum tube) has the function of wireless monitoring. That means the two AH-FBG sensors can provide the temporal variation of θ continuously. Fig. 11 shows the temporal variation of θ at different depths measured from two AH-FBG sensors during about one year (i.e. from 14 March 2021 to 7 February 2022). The water content of the superficial soil, e.g. soil at depths of 0.1 m or 0.12 m, is more prone to fluctuation, as these shallow soil depths are more susceptible to soil-atmosphere interactions. In contrast, soils at deep depth, e.g. 5.1 m or 9.1 m (in Fig. 11b), are unlikely to be affected by external influences and their water content remains relatively stable. However, the DTS demodulator used with AH-DTS sensors lacks an automatic wireless monitoring function, which limits continuous monitoring

Table 5
In situ calibration results using different AHFO sensors.

Parameter	CMHC sensing tube	CFHC sensing tube	CMHC	CFHC	AH-FBG alundum tube	AH-FBG cable
A	0.3205	0.3755	0.71	0.9502	0.2508	0.8044
B	5.5745	4.6835	−0.5934	−3.6266	0.018	8.046
C	0.0247	0.0267	0.0367	0.0425	0.0225	0.0299

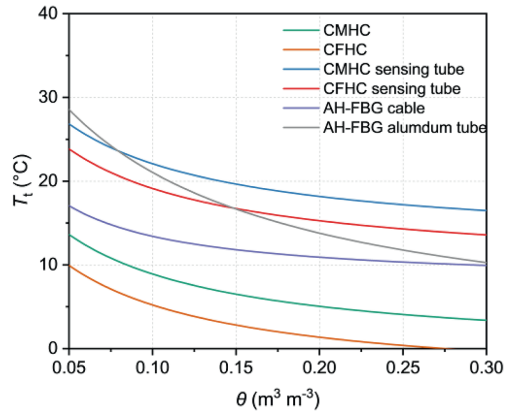

Fig. 9. Calibration curves of in situ results measured by different AHFO sensors.

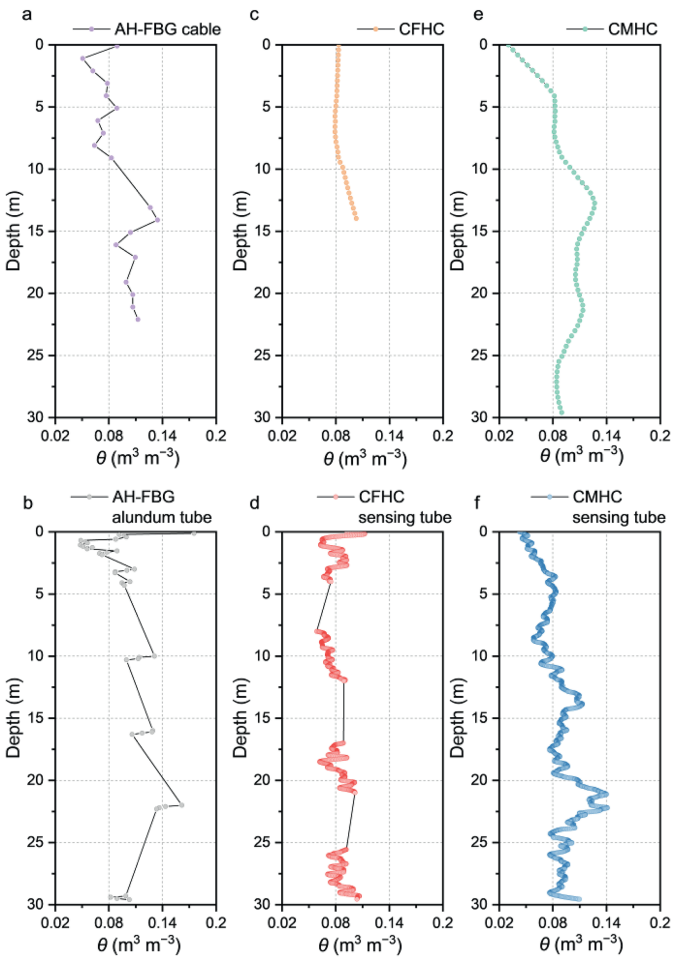

Fig. 10. Spatial distribution of measured θ using different AHFO sensors along depth direction: (a) AH-FBG cable, (b) AH-FBG alundum tube, (c) CFHC, (d) CFHC sensing tube, (e) CMHC, and (f) CMHC sensing tube.

and results in the loss of information regarding the temporal variation of soil water content.

To further evaluate the performance of measurement using different AHFO sensors, the neutron probe access tube is used to measure the soil water content along the depth at the same time. For the quantification of difference between measurements from AHFO sensor and neutron probe access tube, the root mean square error (*RMSE*) is calculated using the following equation:

$$RMSE = \frac{1}{N}\sum_{i=1}^{N}\left(\theta_{\mathrm{AHFO},i} - \theta_{\mathrm{neutron},i}\right)^2 \tag{9}$$

where $\theta_{\mathrm{AHFO},i}$ is the i-th measurement from AHFO sensor, and $\theta_{\mathrm{neutron},i}$ is the i-th measurement from neutron probe access tube at the same depth as $\theta_{\mathrm{AHFO},i}$.

After calculating the *RMSE* of six AHFO sensors using Eq. (9), the results are compared in Fig. 12 for illustration. It is easily observed that the compared results are consistent with the measurement accuracy quantified in numerical simulations, as shown in Fig. 6. The two DTS sensing tubes have the best performance because of the highest heating power per meter. However, CFHC performed well in in situ measurements of soil water content, the same as the CFHC sensing tube, due to the different heating power and complex site conditions. In general, the *RMSE* values of different AHFO sensors in in situ measurement are slightly higher than the quantified measurement accuracy in numerical simulations. This discrepancy arises because certain in situ measurement errors, such as calibration error, measurement noise, and soil moisture migration, which are not accounted for in numerical simulations. Therefore, the in situ measurement results are more reliable for reference, but the numerical simulation results provide an ideal upper limitation of measurement accuracy.

4.4. Evaluation of monitoring potential

In this subsection, a comprehensive analysis of the numerical simulation and in situ measurement results will be provided from various perspectives, comparing the strengths and weaknesses of six different AHFO sensors and assessing their monitoring potential. Evaluation criteria will encompass measurement accuracy, spatio-temporal distribution of soil water content, site conditions, energy support, and some other relevant factors. To illustrate evaluated monitoring potential directly, three different application scenarios are assumed in detail as follows, with determining one or a few proper AHFO sensors for the corresponding scenario.

Scenario I aims to obtain the fine-scale spatial distribution of accurate soil water content in a small-scale site and the site in Scenario I has enough energy for heating the AHFO sensors, e.g. mains electricity. From the in situ measurement results in Section 4.3, the CFHC sensing tube and CMHC sensing tube can not only provide the varying trend of measured soil water content along the tubes, but also measure the θ distribution with highest spatial resolution, i.e. the measurement interval of 0.014 m, because of the distributed sensing from DTS sensors. At the meantime, the measurement accuracy and sensitivity of the CFHC sensing tube and CMHC sensing tube are the highest in the numerical

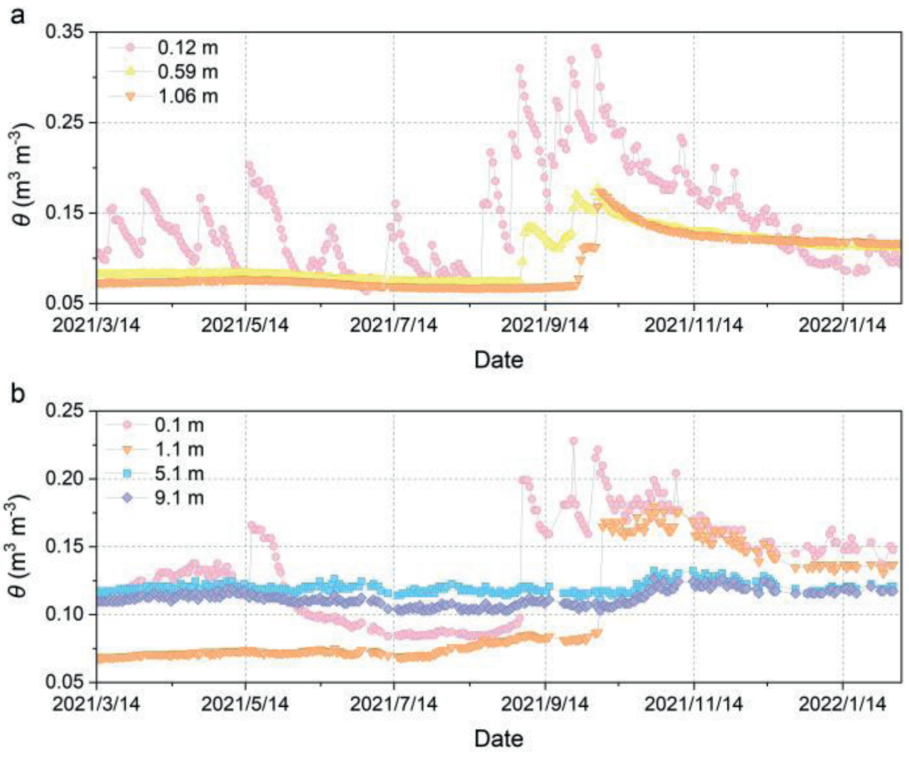

Fig. 11. Temporal variation of measured θ at different depths using two AH-FBG sensors: (a) AH-FBG alundum tube, and (b) AH-FBG cable.

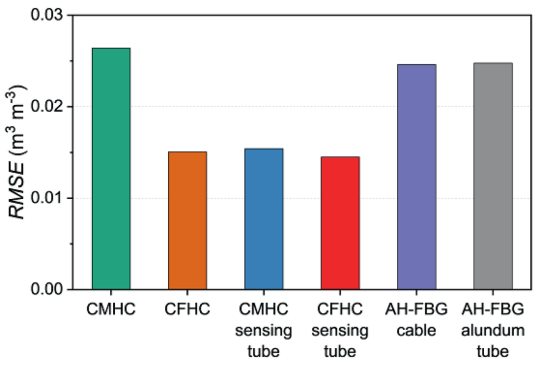

Fig. 12. *RMSE* of measured θ using different AHFO sensors compared with measurements from neutron probe access tube.

simulation. Although the two DTS sensing tubes need large heating power for the measurement, the site in Scenario I is small and can provide enough energy, so that the CFHC sensing tube and CMHC sensing tube are the proper AHFO sensors for Scenario I.

Scenario II aims to obtain a large-scale spatial distribution of soil water content, but the site is far away from the city, so that it can only provide limited energy for heating AHFO sensors, e.g. solar energy. Due to the requirement of large-scale water content distribution, the three cables, i.e. CMHC, CFHC, and AH-FBG cable, are more suitable than the tube-shape sensors. Because of the quasi-distributed sensing technique of FBG, AH-FBG cable is less suitable for this scenario than the other two cables. While the limited providing energy for heating, the CFHC needs large heating power because of the high resistance of carbon fiber. Therefore, the CMHC is the proper AHFO sensor for Scenario II.

Scenario III aims to obtain the spatio-temporal distribution of soil water content of superficial soil. It may focus on the effect of soil-atmosphere interaction on the spatio-temporal distribution of soil water content at the study site. As introduced in Section 4.3, only the two AH-FBG sensors (i.e. AH-FBG cable and AH-FBG alundum tube) have the automatic function of wireless monitoring to provide the long term real-time remote monitoring data. In addition, the Scenario III only cares the soil water content of superficial soil. Considering the sensor size and measurement interval, the AH-FBG alundum tube may be more suitable for Scenario III, because it has high spatio-temporal resolution.

It is well noted that although some sensors, i.e. AH-FBG cable and CFHC, are not recommended in the above three specific scenarios, that only means they are not suitable for these three scenarios and the scenarios are only three special examples. For conveniently determining a proper AHFO sensor, five common

Table 6
Monitoring scenarios with recommended AHFO sensors.

Scenario	Recommended AHFO sensor(s)
Large scale (over 10 m) monitoring	CMHC, CMHC sensing tube
Medium scale (1–10 m) monitoring	CFHC, CFHC sensing tube, AH-FBG cable
Small scale (less than 1 m) monitoring	AH-FBG alundum tube
Real-time remote monitoring	AH-FBG cable, AH-FBG alundum tube
Fine-spatial monitoring	CMHC sensing tube, CFHC sensing tube

Table 7
Monitoring potential of six different AHFO sensors.

Sensor	Measurement accuracy of temperature	Measurement accuracy of water content	Measurement sensitivity	Spatial resolution	Spatial range	Required heating energy	Remote monitoring
AH-FBG cable	High	Medium	Medium	Low	High	Low	Yes
AH-FBG alundum tube	High	Medium	Medium	Low	Low	Low	Yes
CFHC	Medium	Medium	Medium	Medium	Medium	High	No
CMHC	Medium	Medium	Medium	Medium	High	Low	No
CFHC sensing tube	Medium	High	High	High	Medium	High	No
CMHC sensing tube	Medium	High	High	High	High	Medium	No

scenarios are summarized with recommended AHFO sensors in Table 6. There are multiple scenarios in the real world for different applications of AHFO sensors. Furthermore, the monitoring potential of six AHFO sensors used in this study are summarized in Table 7, including the measurement accuracy of temperature, measurement accuracy of water content, measurement sensitivity, spatial resolution, spatial range, required heating energy, and ability of real-time monitoring. When determining the AHFO sensor for a specific application, this table can provide a helpful reference for the geotechnical engineers or researchers.

5. Conclusions

To assess the measurement performance and monitoring potential of various AHFO sensors, in this study, numerical simulations and in situ tests of soil water content measurements by six different AHFO sensors were conducted, respectively. Firstly, the temperature variations of the six types of AHFO sensors under different soil water content conditions were obtained through numerical simulations using the same heating pulse. Then, T_t-θ calibration formulae were established to evaluate the measurement accuracy and measurement sensitivity of soil water content measured by each AHFO sensor. Subsequently, these six AHFO sensors were deployed in the same test pit, and the spatial and temporal distribution of soil water content measured by each AHFO sensor was obtained through in situ monitoring tests. A comparative analysis was conducted on the advantages and disadvantages of the field applications by these six AHFO sensors. Finally, comprehensive evaluations of the water content measurement performance and in situ application potential were analyzed based on numerical simulation and in situ application results. The conclusions drawn from this study are as follows:

(1) When evaluating the measurement accuracy, CFHC sensing tube and CMHC sensing tube demonstrate the highest performance (less than 0.005 m^3 m^{-3}), followed by AH-FBG alundum tube and AH-FBG cable (less than 0.01 m^3 m^{-3}), with CFHC and CMHC being the lowest (about 0.015 m^3 m^{-3}). In terms of measurement sensitivity, CFHC sensing tube and CMHC sensing tube exhibit the strongest response (about 80 °C per unit water content), while the remaining four sensors (CFHC, AH-FBG cable, CMHC, and AH-FBG alundum tube) show significantly lower sensitivity (about 20 °C per unit water content).
(2) The CFHC sensing tube and CMHC sensing tube possess higher spatial resolutions (about 0.035 m) compared to the 1 m resolution of CFHC and CMHC, rendering them more suitable for detailed characterization of soil water content.
(3) The CMHC sensing tube, with a low electrical resistance of 0.018 Ω m^{-1}, is more suitable for soil water content monitoring in deep hole compared to the CFHC sensing tube.
(4) Combined with FBG wireless demodulator, the AH-FBG alundum tube and AH-FBG cable can provide remote real-time measurements, thereby enabling long-term in situ water content monitoring.
(5) In the actual selection and application of AHFO sensors, it is recommended to choose the appropriate AHFO sensors based on monitoring objectives, considering factors such as water content measurement performance, spatial resolution of sensors, monitoring duration, site installation, and power supply conditions.

In the future, priority will be given to investigating the applicability of AHFO sensors across varied scenarios in order to standardize their in situ application. Meanwhile, the development of new AHFO sensors with advanced designs is necessary to meet complex field challenges.

CRediT authorship contribution statement

Mengya Sun: Writing – review & editing, Data curation, Funding acquisition, Investigation, Writing – original draft, Conceptualization, Validation. **Juncheng Yao:** Writing – review & editing, Data curation, Methodology, Software, Validation, Writing – original draft, Formal analysis. **Jie Liu:** Investigation, Methodology, Software, Data curation. **Jin Liu:** Project administration, Resources. **Yuling Xin:** Conceptualization, Investigation, Validation. **Bin Shi:** Project administration, Writing – review & editing, Conceptualization, Supervision.

Declaration of competing interest

The authors declare that they have no known competing financial interests or personal relationships that could have appeared to influence the work reported in this paper.

Acknowledgments

This work was supported by the National Natural Science Foundation of China (Grant No. 42307189) and the China Postdoctoral Science Foundation (Grant Nos. 2024T170215 and 2023M740974).

References

Benítez-Buelga, J., Rodríguez-Sinobas, L., Calvo, R.S., Gil-Rodríguez, M., Sayde, C., Selker, J.S., 2016. Calibration of soil moisture sensing with subsurface heated fiber optics using numerical simulation. Water Resour. Res. 52, 2985e2995.
Bao, Y., Chen, G., 2016. Temperature-dependent strain and temperature sensitivities of fused silica single mode fiber sensors with pulse pre-pump Brillouin optical time domain analysis. Meas. Sci. Technol. 27, 065101.
Bao, Y., Huang, Y., Hoehler, M.S., Chen, G., 2019. Review of fiber optic sensors for structural fire engineering. Sensors 19 (4), 877.
Bittelli, M., Ventura, F., Campbell, G.S., Snyder, R.L., Gallegati, F., Pisa, P.R., 2008.

Coupling of heat, water vapor, and liquid water fluxes to compute evaporation in bare soils. J. Hydrol. 362, 191e205.
Bristow, K.L., White, R.D., Kluitenberg, G.J., 1994. Comparison of single and dual probes for measuring soil thermal properties with transient heating. Soil Res. 32, 447e464.
Cao, D., Shi, B., Zhu, H., Wei, G., Chen, S.E., Yan, J., 2015. A distributed measurement method for in situ soil moisture content by using carbon-fiber heated cable. J. Rock Mech. Geotech. Eng. 7 (6), 700e7.
Cao, D., Shi, B., Zhu, H., Zhu, K., Wei, G., Gu, K., 2016. Performance evaluation of two types of heated cables for distributed temperature sensing-based measurement of soil moisture content. J. Rock Mech. Geotech. Eng. 8, 212e217.
Ciocca, F., Lunati, I., Van de Giesen, N., Parlange, M.B., 2012. Heated optical fiber for distributed soil-moisture measurements: a Lysimeter experiment. Vadose Zone J. 11 (4), vzj2011, 0199.
Gil-Rodríguez, M., Rodríguez-Sinobas, L., Benítez-Buelga, J., Sanchez-Calvo, R., 2013. Application of active heat pulse method with fiber optic temperature sensing for estimation of wetting bulbs and water distribution in drip emitters. Agric. Water Manag. 120, 72e78.
Guo, J., Sun, M., Shi, B., Wei, G., Liu, J., 2020. Experimental study of water content in soils monitored with active heated fiber optic method at different ambient temperatures. Rock Soil Mech. 41, 4137–4144.
Heitman, J.L., Xiao, X., Horton, R., Sauer, T.J., 2008. Sensible heat measurements indicating depth and magnitude of subsurface soil water evaporation. Water Resour. Res. 44. https://doi.org/10.1029/2008WR006961.
Kluitenberg, G.J., Ham, J.M., Bristow, K.L., 1993. Error analysis of the heat pulse method for measuring soil volumetric heat capacity. Soil Sci. Soc. Am. J. 57, 1444e1451.
Li, J., Zhu, H.H., Wu, B., Hu, L.L., Liu, X.F., Shi, B., 2023. Study on actively heated fiber Bragg grating sensing technology for expansive soil moisture considering the influence of cracks. Measurement 218, 113087.
Liu, J., Che, W., Lan, X., et al., 2023. Performance and mechanism of a novel biopolymer binder for clayey soil stabilization: mechanical properties and microstructure characteristics. Transp. Geotech. 42, 101044.
Liu, J., Cui, Y.J., Sun, M.Y., Gu, K., Yao, J.C., Tang, C.S., Shi, B., 2024a. Field investigation of unsaturated hydraulic conductivity using actively heated fiber-optic technology. J. Hydrol. https://doi.org/10.1016/j.jhydrol.2024.131596.
Liu, J., Shi, B., Cui, Y.J., Sun, M.Y., Gu, K., Yao, J.C., Tang, C.S., 2024b. Predicting the deformation of compacted loess used for land creation based on the field monitoring with fiber-optic technology. Eng. Geol. 336, 107542.
Phoon, K.-K., Kulhawy, F.H., 1999. Characterization of geotechnical variability. Can. Geotech. J. 36, 612–624.
Qin, Z., Qu, S., Wang, Z., Yang, W., Li, S., Liu, Z., Xu, Y., 2022. A fully distributed fiber optic sensor for simultaneous relative humidity and temperature measurement with polyimide-coated polarization maintaining fiber. Sensors Actuators B Chem. 373, 132699.
Sayde, C., Gregory, C., Gilrodriguez, M., et al., 2010. Feasibility of soil moisture monitoring with heated fiber optics. Water Resour. Res. 46, 2840e2849.
Sayde, C., Buelga, J.B., Rodriguez-Sinobas, L., El Khoury, L., English, M., van de Giesen, N., Selker, J.S., 2014. Mapping variability of soil water content and flux across 1e1000 m scales using the actively heated fiber optic method. Water Resour. Res. 50, 7302e7317.
Sayde, C., Thomas, C.K., Wagner, J., Selker, J., 2015. High-resolution wind speed measurements using actively heated fiber optics. Geophys. Res. Lett. 42 (22), 10,064-10,073.
Sourbeer, J.J., Loheide, S.P., 2016. Obstacles to long-term soil moisture monitoring with heated distributed temperature sensing. Hydrol. Process. 30, 1017e1035.
Striegl, A.M., Loheide II, S.P., 2012. Heated distributed temperature sensing for field scale soil moisture monitoring. Groundwater 50, 340e347.
Sun, M.Y., Shi, B., Zhang, D., Liu, J., Guo, J.Y., Wei, G.Q., Chang, W., 2020. Study on calibration model of soil water content based on actively heated fiber-optic FBG method in the in situ test. Measurement 165, 108176.
Sun, M., Shi, B., Zhang, C., Zheng, X., Guo, J., Wang, Y., et al., 2021. Quasi-distributed fiber-optic in situ monitoring technology for large-scale measurement of soil water content and its application. Eng. Geol. 294, 106373.
Sun, M., Wu, P., Shi, B., Liu, J., Liu, J., Yao, J., et al., 2024a. AHFO-based soil water content sensing technology considering soil–sensor thermal contact resistance. J. Rock Mech. Geotech. Eng. 16 (7), 2715–2731.
Sun, M., Liu, J., Liu, J., Zheng, X., Li, X., Guo, J., Wang, Y., Tong, Y., Shi, B., 2024b. Development and in situ application of actively heated fiber Bragg grating cable for soil water content measurement. J. Rock Mech. Geotech. Eng. https://doi.org/10.1016/j.jrmge.2024.09.033.
Taylor, S.A., Cavazza, L., 1954. The movement of soil moisture in response to temperature gradients. Soil Sci. Soc. Am. Proc. 18, 351–358.
Wang, M., Li, X., Chen, L., Hou, S., Wu, G., Deng, Z., 2020. A modified soil water content measurement technique using actively heated fiber optic sensor. J. Rock Mech. Geotech. Eng. 12 (3), 608e619.
Wu, B., Zhu, H.H., Cao, D., Xu, L., Shi, B., 2021. Feasibility study on ice content measurement of frozen soil using actively heated FBG sensors. Cold Reg. Sci. Technol. 189, 103332.
Wu, B., Zhu, H.H., Cao, D.F., Liu, X.F., Liu, T.X., 2023. Fiber optic sensing-based field investigation of thermo-hydraulic behaviors of loess for characterizing land-atmosphere interactions. Eng. Geol. 315, 107019.
Yao, J.C., Shi, B., Liu, J., Sun, M.Y., Fang, K., Yao, J., Gu, K., Zhang, W., Zhang, J.W., 2022. Improvement and performance evaluation of a dual-probe heat pulse distributed temperature sensing method used for soil moisture estimation. Sensors 22, 7592.
Yao, J.C., Liu, J., Wang, J.L., Sun, M.Y., Fang, K., Shi, B., 2023. A study of soil thermal conductivity measurement based on the actively heated distributed temperature sensing cable. Hydrogeol. Eng. Geol. 50 (1), 179–188. https://doi.org/10.16030/j.cnki.issn.1000-3665.202111076.
Zhang, B., Gu, K., Shi, B., Liu, C., Bayer, P., Wei, G., et al., 2020. Actively heated fiber optics based thermal response test: a field demonstration. Renew. Sustain. Energy Rev. 134, 110336.
Zhang, B., Gu, K., Wang, B., Zhao, P., Shi, B., 2023. Sensitivity study of thermal response test using resistively heated methods under various setups. Measurement 219, 113284.

Bin Shi received his PhD from Nanjing University in 1995. He is a professor and a doctoral supervisor in the School of Earth Sciences and Engineering at Nanjing University, China. He has been engaged in research on soil and rock disasters in the fields of geotechnical engineering and geological engineering. He has published more than 200 SCI papers which have been cited more than 6500 times, with the highest citation for a single SCI paper being 629 times. He has been awarded 76 national authorized invention patents and served as the chief editor for 2 national industry association standards. He has received a first prize of the National Scientific and Technology Progress Award ranking the first, and other 10 provincial or ministerial awards in natural science, invention, and scientific and technology progress.